

VIMS Articles

2015

In situ phytoplankton distributions in the Amundsen Sea Polynya measured by autonomous gliders

O Schofield

T Miles

AC Alderkamp

S Lee

C Haskins

See next page for additional authors

Follow this and additional works at: <https://scholarworks.wm.edu/vimsarticles>



Part of the [Aquaculture and Fisheries Commons](#)

Recommended Citation

Schofield, O; Miles, T; Alderkamp, AC; Lee, S; Haskins, C; Rogalsky, E; Sipler, R; Sherrell, RM; and Yager, PL, "In situ phytoplankton distributions in the Amundsen Sea Polynya measured by autonomous gliders" (2015). *VIMS Articles*. 827.

<https://scholarworks.wm.edu/vimsarticles/827>

This Article is brought to you for free and open access by W&M ScholarWorks. It has been accepted for inclusion in VIMS Articles by an authorized administrator of W&M ScholarWorks. For more information, please contact scholarworks@wm.edu.

Authors

O Schofield, T Miles, AC Alderkamp, S Lee, C Haskins, E Rogalsky, R Sipler, RM Sherrell, and PL Yager



In situ phytoplankton distributions in the Amundsen Sea Polynya measured by autonomous gliders

Oscar Schofield^{1*} • Travis Miles¹ • Anne-Carlijn Alderkamp² • SangHoon Lee³ • Christina Haskins¹ • Emily Rogalsky¹ • Rachel Sipler⁴ • Robert M. Sherrell^{1,5} • Patricia L. Yager⁶

¹Center for Ocean Observing Leadership, Department of Marine and Coastal Sciences, School of Environmental and Biological Sciences, Rutgers University, New Brunswick, New Jersey, United States

²Department of Environmental Earth System Science, Stanford University, Stanford, California, United States

³Korea Polar Research Institute, YonSu-Ku, Incheon, Korea

⁴Virginia Institute of Marine Science, College of William & Mary, Gloucester Point, Virginia, United States

⁵Department of Earth and Planetary Sciences, Rutgers University, Piscataway, New Jersey, United States

⁶Department of Marine Sciences, University of Georgia, Athens, Georgia, United States

*oscar@marine.rutgers.edu

Abstract

The Amundsen Sea Polynya is characterized by large phytoplankton blooms, which makes this region disproportionately important relative to its size for the biogeochemistry of the Southern Ocean. *In situ* data on phytoplankton are limited, which is problematic given recent reports of sustained change in the Amundsen Sea. During two field expeditions to the Amundsen Sea during austral summer 2010–2011 and 2014, we collected physical and bio-optical data from ships and autonomous underwater gliders. Gliders documented large phytoplankton blooms associated with Antarctic Surface Waters with low salinity surface water and shallow upper mixed layers (< 50 m). High biomass was not always associated with a specific water mass, suggesting the importance of upper mixed depth and light in influencing phytoplankton biomass. Spectral optical backscatter and ship pigment data suggested that the composition of phytoplankton was spatially heterogeneous, with the large blooms dominated by *Phaeocystis* and non-bloom waters dominated by diatoms. Phytoplankton growth rates estimated from field data ($\leq 0.10 \text{ day}^{-1}$) were at the lower end of the range measured during ship-based incubations, reflecting both *in situ* nutrient and light limitations. In the bloom waters, phytoplankton biomass was high throughout the 50-m thick upper mixed layer. Those biomass levels, along with the presence of colored dissolved organic matter and detritus, resulted in a euphotic zone that was often < 10 m deep. The net result was that the majority of phytoplankton were light-limited, suggesting that mixing rates within the upper mixed layer were critical to determining the overall productivity; however, regional productivity will ultimately be controlled by water column stability and the depth of the upper mixed layer, which may be enhanced with continued ice melt in the Amundsen Sea Polynya.

Introduction

The Southern Ocean is disproportionately important to the global biogeochemical system, accounting for up to half of the annual oceanic uptake of anthropogenic carbon dioxide (CO₂) from the atmosphere (Arrigo et al., 2008; Gruber et al., 2009). Models suggest that the vertical mixing there supplies enough nutrients to fertilize three-quarters of the biological production in the global ocean north of 30°S (Sarmiento et al., 2004). Given the large-scale documented changes being observed in many sectors of the Southern Ocean gaining a better understanding of the biogeochemical dynamics is critical (Ducklow et al., 2007; Schofield et al., 2010).

One region showing dramatic change is the Amundsen Sea, which is influenced by some of the largest and most rapid glacier melt and ice sheet thinning in the Southern Ocean (Rignot, 2008). The Amundsen

Domain Editor-in-Chief

Jody W. Deming, University of Washington

Associate Editor

Jean-Éric Tremblay, Université Laval

Knowledge Domain

Ocean Science

Article Type

Research Article

Part of an *Elementa* Special Feature

ASPIRE: The Amundsen Sea Polynya International Research Expedition

Received: September 17, 2014

Accepted: September 15, 2015

Published: October 14, 2015

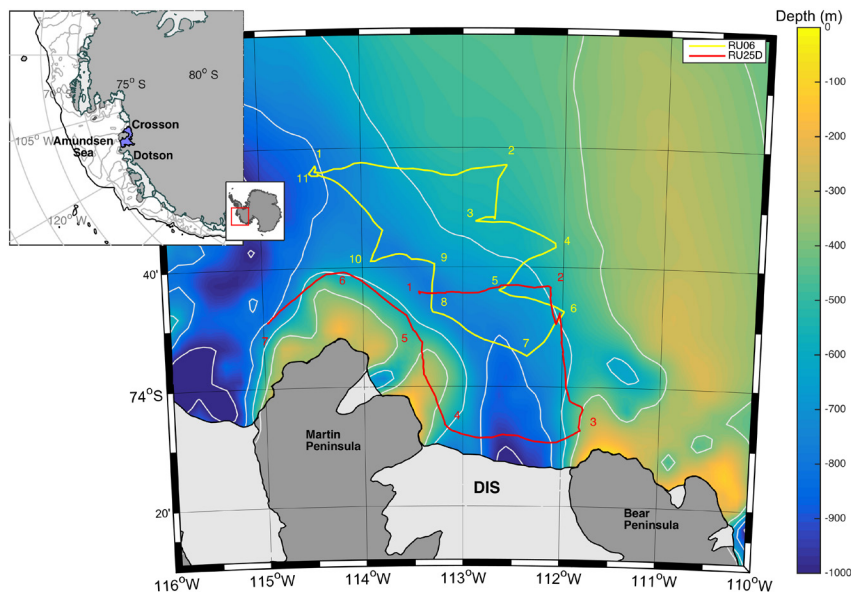


Figure 1

Map of the study area for the ASPIRE and KOPRI cruises.

The Amundsen Sea located near the Dotson and Crosson Ice shelves shown in blue on the inset map (adapted from Rignot et al., 2013). Colored lines indicate the glider missions: yellow for the glider mission during ASPIRE, red for the glider mission during the KOPRI cruise. Numbers on the lines are used to delineate different segments of a glider transect. Depths are indicated by the blue color scale and contour lines, the Antarctic continent is dark gray, and the ice shelves are light gray.

doi: 10.12952/journal.elementa.000073.f001

Sea (Figure 1) harbors two particularly productive polynyas, the Amundsen Sea Polynya (ASP) with an area of $\sim 27,000$ km² and the Pine Island Polynya at $\sim 18,000$ km² (Arrigo et al., 2012). The ASP is a perennially occurring latent heat polynya (Arrigo et al., 2012), though there are indications of a significant sensible component (Stammerjohn et al., 2015). A small portion appears to remain ice-free in winter, but in November it begins to expand, reaching a mean maximum opening in February, after which it rapidly closes in March. In the ASP, the length of the sea ice season has declined by 60 ± 9 days since 1979, a change largely due to the ASP opening earlier in the year by 52 ± 9 days (Arrigo et al., 2012). The shorter sea ice season facilitates increased solar ocean warming, leading to greater sea ice declines. The loss is hypothesized to reflect a poleward intensification of the prevailing storm tracks in the Amundsen-Bellingshausen Sea region (Marshall, 2007; Stammerjohn et al., 2012).

Changes in the Amundsen Sea have significant biological and chemical implications (Yager et al., 2012). The ASP is one of the most productive polynyas (per unit area) in the Antarctic (Arrigo and van Dijken, 2003). Satellite-derived seasonally averaged chlorophyll *a* levels (2.2 ± 3.0 mg m⁻³) are 40% greater than the Ross Sea Polynya (RSP; 1.5 ± 1.5 mg m⁻³). Primary productivity in Southern Ocean polynyas tends to be dominated by prymnesiophytes (*Phaeocystis antarctica*) or diatoms (Arrigo et al., 2008). The relative contributions of prymnesiophytes and diatoms reflect a complex interplay of physical circulation/mixing conditions, the light environment, and concentrations of macro- and micro-nutrients. A better understanding of the physical forcing of these communities is important because community composition has biogeochemical implications and this regional system is changing (Arrigo et al., 1999; Alderkamp et al., 2012; Fragoso and Smith, 2012). For example, *P. antarctica* takes up twice as much CO₂ per mole of phosphate removed as diatoms (Arrigo et al., 1999), it is not a preferred prey of microzooplankton (Caron et al., 2000), and its presence has been linked to dimethyl sulfide cycling between the ocean and atmosphere (Liss et al., 1994). The processes driving local productivity and community composition are affected by local weather, which results in high interannual variability in the phytoplankton concentrations (Smith et al., 2006). In the ASP, the interannual variability is higher (138%) than in the RSP (101%) (Arrigo and van Dijken, 2003), emphasizing the critical need to better understand the links between the physical environment of the Amundsen Sea region and the corresponding response in the phytoplankton communities.

Autonomous technologies, which have matured greatly over the last decade, provide means for sampling temporal and spatial domains that are difficult to resolve using traditional ship-based sampling (Davis et al., 2003; Schofield et al., 2007). Underwater Slocum gliders are effective at measuring a wide range of physical (temperature, salinity, currents; Schofield et al., 2007), chemical (oxygen) and bio-optical properties (spectral optical backscatter, chlorophyll fluorescence, colored dissolved organic fluorescence; Schofield et al., 2007; Glenn et al., 2008). Slocum gliders have proven to be effective at characterizing high-resolution horizontal scales, from tens of meters to thousands of kilometers with vertical resolutions < 1 m, and are important tools for studying physical/particle interactions in marine systems (Glenn et al., 2008; Rudnick and Cole, 2011; Miles et al., 2012; Xu et al., 2012; Schofield et al., 2013a).

Physical and bio-optical data were collected using both ship and gliders during two separate field expeditions to the Amundsen Sea. The combined data from both expeditions were used to assess commonalities in the phytoplankton distributions in the polynya. Both expeditions document that high phytoplankton

biomass is associated with stratified, shallow, upper mixed layer depths, suggesting the critical role of light in promoting phytoplankton blooms.

Materials and methods

Data were collected during two expeditions to the Amundsen Sea in the South Pacific sector of the Southern Ocean in 2010 and 2013 (Figure 1). The majority of the data was collected during the 2010 field season of the Amundsen Sea Polynya International Research Expedition (ASPIRE; Yager et al., 2012). ASPIRE was conducted as part of the International Polar Year onboard the RVIB *Nathaniel B. Palmer* (NBP) chartered by the US National Science Foundation through its Antarctic Program. The primary objective of the ASPIRE program was to investigate the climate-sensitive processes driving the productivity and carbon sequestration of the ASP. The second data set was collected in January of 2014 as part of the ANA04B cruise of the Korean Polar Research Institute (KOPRI) onboard the IBRV Araon. This effort was conducted in the same area as ASPIRE, with a goal to understand regional circulation and corresponding impacts on Amundsen Sea biogeochemistry.

For both expeditions, discrete sampling was conducted with a CTD rosette outfitted with Niskin bottles allowing for water collection. In this paper we focus on the discrete data from the ASPIRE expedition. During ASPIRE, water was sampled with 12-L bottles from discrete depths in the upper 300 m of the water column at 19 stations (Sherrell et al., 2015). Continuous vertical profiles of temperature, salinity, irradiance, fluorescence, and beam attenuation were obtained from the water column using a SeaBird 911+ CTD, a Chelsea fluorometer, photosynthetically active radiation (PAR) sensor (Biospherical Instruments), and a 25-cm WetLabs transmissometer, mounted on a conventional rosette, deployed using a kevlar cable and winch. Discrete water samples were analyzed for chlorophyll *a* and phytoplankton accessory pigments. Chlorophyll *a* samples were filtered onto 25 mm Whatman GF/F filters, extracted overnight in 5 ml of 90% acetone, and analyzed on a Turner Model 10AU fluorometer before and after acidification (Holm-Hansen et al., 1965). High pressure liquid chromatography (HPLC) analyses were conducted on discrete samples to provide estimates of the chlorophylls and carotenoids. For the HPLC samples, 0.1–2 L were filtered onto 25 mm Whatman GF/F filters, flash-frozen in liquid nitrogen, and stored at -80°C until analysis on a Shimadzu system according to Wright et al. (1991). Chlorophyll *a* measurements on the discrete samples at the time of glider deployments (see below) were considered the “correct values” and used to adjust fluorometric estimates of chlorophyll *a*. Given the relatively short deployment times (just under two weeks) we assume that bio-fouling was negligible.

During both of these expeditions, Webb Slocum gliders (Schofield et al., 2007) were deployed to provide high-resolution surveys of the physical and bio-optical properties near the ice edge (Figure 1). Slocum gliders are autonomous buoyancy-driven vehicles. These 1.5 m long platforms maneuver up and down within the water column through the ocean at a forward speed of $20\text{--}30\text{ cm s}^{-1}$ in a sawtooth-shaped gliding trajectory by means of a buoyancy change, where wings translate the sinking motion, due to gravity, into the forward direction. A tail fin rudder provides the steering. The forward navigation system of the vehicle is based on an onboard GPS receiver coupled with an attitude sensor, depth sensor and altimeter. This configuration allows for “dead-reckoning” navigation to a designated waypoint based on the desired target location. Additionally the altimeter and depth sensor allow scientists to program the sampling in the water column. Global iridium phones embedded within the glider tails are periodically raised out of the water when the vehicle sits at the surface at predetermined intervals. Once at the surface, the glider retrieves its position, transmits data to shore, and checks for any programmed changes to the mission. For the gliders, sensor data are logged every 2 seconds on downcast and upcast as it travels with vertical speeds of 20 cm s^{-1} , resulting in high data density relative to traditional shipboard sampling. The gliders used in this study were G2 gliders equipped with a suite of oceanographic sensors. This suite included three science sensors: a Seabird unpumped conductivity temperature and depth (CTD) sensor, a Wetlabs triplet sensor, and an Aanderaa oxygen Optode. While a pumped CTD is preferred to minimize any thermal lag associated with the conductivity cell, none was available for these efforts; however, there was no evidence of salinity spiking, suggesting no bias in the derived salinity values resulting from thermal inertia. Prior to and after deployment, the glider CTD was compared to independent CTDs in a tank test, and the results indicated that the glider CTD did not exhibit any drift.

The pre- and post-dive latitude and longitude of the glider, along with glider pitch, heading, and vertical velocity, were combined to calculate dead-reckoned currents (Davis et al., 2003). The horizontal velocity of the glider was estimated using simple geometry by combining the systems-measured pitch angle and the vertical velocity calculated from the change in pressure with time, while the glider compass was used to determine heading. The instantaneous horizontal velocities were integrated in time for the duration of the glider dive time to obtain an estimated glider position independent of ambient currents. The difference between the estimated surfacing position and actual position divided by the duration of the dive results in a time- and depth-integrated, dead-reckoned water column velocity. The largest source of error in this method of current calculation is the calibration of the glider compass. Both RU06 and RU25D compasses were calibrated

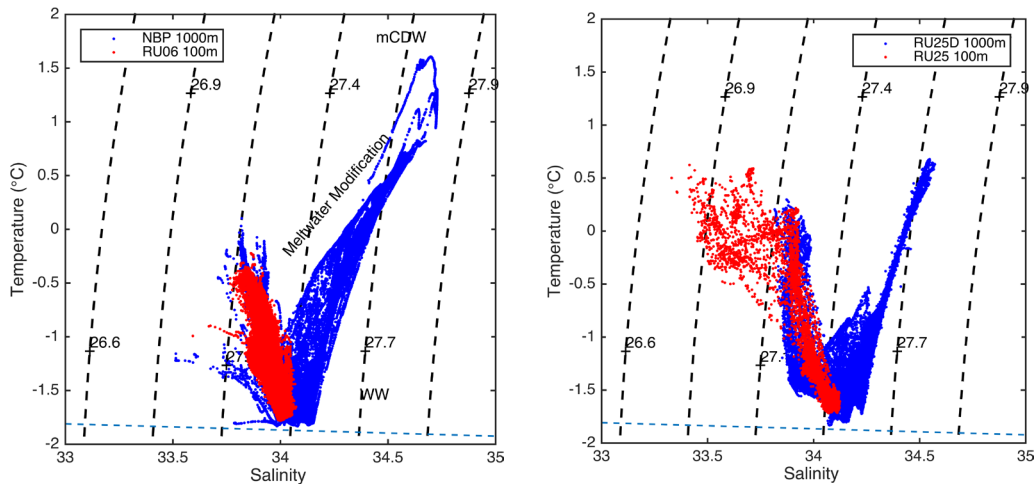


Figure 2

Temperature and salinity properties measured during the ASPIRE and KOPRI cruises.

Shown in (A) are the temperature and salinity properties measured during ASPIRE in austral summer of 2010–2011 using both the CTD from the ship (NBP) over the full 1000-m water column (blue) and the glider (RU06) which profiled only the upper 100 m (red). Glider data from the KOPRI cruise in austral summer of 2013–2014 are shown in (B) where blue indicates glider data for the full water column (RU25D) and red indicates glider data from the upper 100 m (RU25). Side by side casts of the ship CTDs and the gliders showed that both measured the same features in the water column, as shown for ASPIRE data in (A). Glider measurements for temperature were lower than the CTD by 0.05°C . Glider measurements for salinity were lower than the CTD by 0.01. We took the ship CTD data as correct and adjusted the glider measurements by those offsets.

doi: 10.12952/journal.elementa.000073.f002

following manufacturer specifications and checked using an 8-point heading test prior to deployment. This dead-reckoned current estimation method has been used extensively in a range of conditions (Glenn et al., 2008; Merckelbach et al., 2008; Miles et al., 2012, 2015a) and has been shown to perform well compared to moored acoustic Doppler current profilers (Davis et al., 2003).

In order to assess the influence of tidal velocities on glider currents for each deployment, we extracted all ten tidal constituents from the Circum-Antarctic Tidal Simulation Model (CATS2008b) (Padman et al., 2002) in the vicinity of the deployments (74°S and 112.5°W). CATS2008b represents the barotropic tidal velocities and has been used in previous studies in the Amundsen Sea Polynya (Wählin et al., 2010, 2012; Assmann et al., 2013; Ha et al., 2014).

ASPIRE took place between 25 November 2010 and 18 January 2011. Two glider deployments were conducted while in the ASP; the first mission (Dec 15–28) covered 300 km in 13 days. The glider was recovered and redeployed for a second shorter deployment (Jan 01–05) covering 75 km in 3.5 days. The glider for this mission (RU06) was outfitted with a 200-m buoyancy pump and a non-pumped SBE41cp Seabird Conductivity-Temperature sensor, though it only profiled in the upper 100 m of the water column. There was good agreement between the glider and ship rosette temperature and salinity data (Figure 2). The glider was also equipped with two WET Labs Environmental Characterization Optics (ECO) pucks. The ECO pucks measured chlorophyll *a* fluorescence, colored dissolved organic matter (CDOM) fluorescence and optical backscatter at 470, 532, and 660 nm. The CDOM fluorometer was outfitted with an excitation wavelength of 370 nm and emission wavelength of 460 nm, with the sensor having a sensitivity of 0.09 ppb. The ECO Pucks were factory-calibrated prior to deployments. The backscatter measurements were measured at 117° degrees, the angle determined as a minimum convergence point for variations in the volume-scattering function induced by suspended materials and water itself. We converted from the volume-scattering function to estimated backscatter coefficients following Boss and Pegau (2001). As a result, the signal measured was less determined by the type and size of the materials in the water and more directly correlated to the concentration of the materials.

For the KOPRI expedition (27 December 2013 – 18 January 2014), the RU25D glider was outfitted with a 1000-m pump, a non-pumped SBE41cp Seabird Conductivity-Temperature sensor, a single WET Labs puck configured to make measurements of optical backscatter at 470 and 532 nm, along with chlorophyll *a* and CDOM fluorescence and an Aandeara oxygen optode. This deep-water glider conducted a 234-km mission over 9 days (04–14 January 2014).

Ship-based ocean currents during ASPIRE were measured with a ‘narrow beam’ 150-kHz and ‘Ocean Surveyor’ 38-kHz hull mounted Acoustic Doppler Current Profilers (ADCP) from Teledyne RD Instruments, Inc. The ADCP data were calibrated and post-cruise corrected by the University of Hawaii. The Teledyne instrument provides accurate data to a depth of 400 m, while the Ocean Surveyor data cover a larger depth range but with coarser vertical resolution.

Ocean color imagery was obtained from the National Aeronautics and Space Administration (NASA) Moderate Resolution Imaging Spectroradiometer (MODIS) onboard the polar orbiting Aqua satellite. The products used here are the standard level-3 mapped 8-day composites for chlorophyll *a* (obtained from <http://oceancolor.gsfc.nasa.gov/>). Typically for these waters, satellite-derived chlorophyll concentrations tend to be under-estimated (Johnson et al., 2013); therefore, these maps should be considered lower limit estimates.

The mean satellite-derived chlorophyll fields, as well as the integrated water column chlorophyll data measured by the gliders, were used as inputs to the Hydrolight 4.3 radiative transfer model (Mobley, 1994) to estimate optical properties within the water. For the Hydrolight simulations, we used default settings and

assumed a constant backscatter to total scatter ratio of 0.005. We assumed there was no inelastic scattering and kept wind speeds at zero. The surface flux of light was calculated using a semi-empirical sky model (Mobley, 1994) at local noon on a cloudless day. We assumed that the water column was infinitely deep. For these simulations we treated these waters as Case I waters (Mobley et al., 1994).

Results

Water masses and flows along the ice sheet in the Amundsen Polynya

Ship and glider surveys encountered three major water masses in this region: Antarctic Surface Water (AASW), Winter Water (WW), and modified Circumpolar Deep Water (mCDW). AASW was observed by ships and gliders during both ASPIRE and KOPRI cruises (Figure 2). It ranged in thickness from ~ 5 to 80 m and was characterized by low salinity (< 34.1), presumably freshened by sea ice melt, and by a temperature range of -1.8 to $> 0^{\circ}\text{C}$ (Figures 3, 4). The glider encountered, at lower latitudes, low salinity surface water (salinity values reduced by ≥ 0.3) (Figure 3, 4). Cold ($< -1.7^{\circ}\text{C}$) WW, with a well-defined salinity value (34.14) reflecting sea ice growth during the previous winter, was typically found extending either from the surface or from the AASW layer down to 300–400 m depth (Figure 4). The warmer (0.6 to 1.2°C) and saltier (34.5 to 34.7) mCDW was observed by RU25D, with warmest temperatures encountered below 600 m (Figure 4A, 5A). Regions with low surface salinity generally had homogeneous mixed layers with a stratified region at base over the WW. We defined the upper stratified layer by the depth of the highest water column buoyancy frequency (N^2). The upper mixed layer ranged from 20 to 80 m in depth (Figures 3D, 4D, 5D). Highest chlorophyll was associated with water columns when the N^2 was shallower than 50 m. During ASPIRE the shallow upper mixed layers and highest chlorophyll were associated with regions of lower surface salinity. During the KOPRI effort the shallow upper mixed layers and highest chlorophyll were associated with regions of warm surface waters (0.0 – 0.5°C). Possible reasons for these differences might reflect the general position of the glider missions, as the KOPRI glider surveyed directly adjacent the outflow at the ice edge while the ASPIRE glider surveyed further offshore in the polynya potentially allowing for radiant heating as the water flowed offshore (Figure 1).

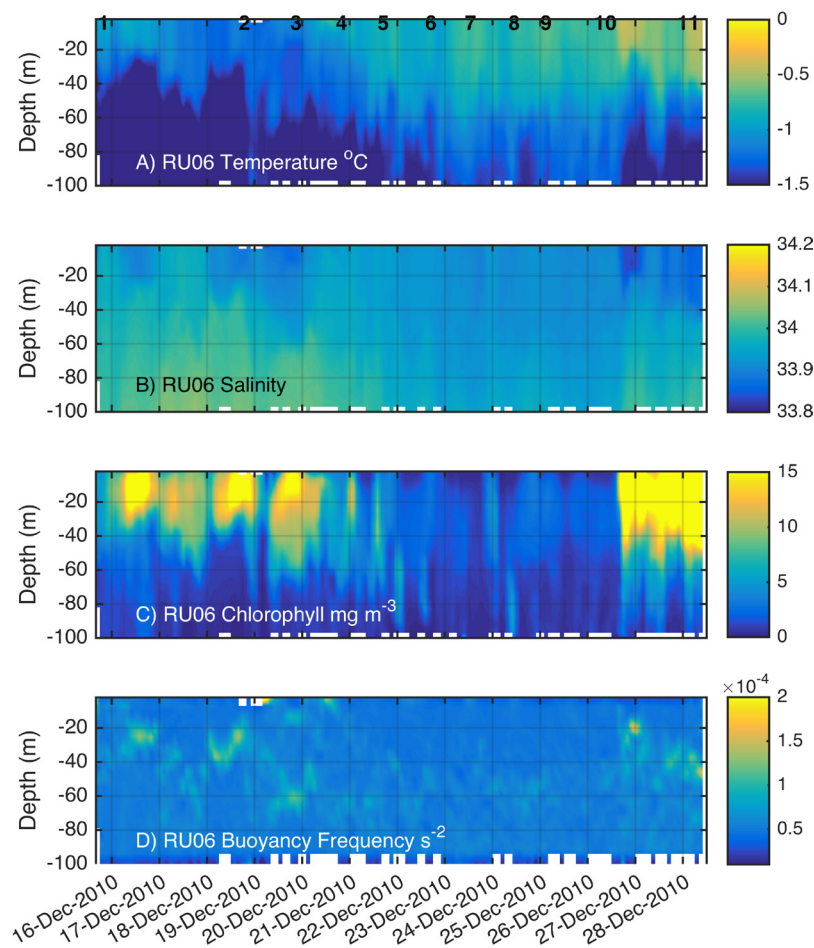


Figure 3

The water column data collected by the Webb Slocum glider during the ASPIRE cruise.

Temperature, salinity, chlorophyll fluorescence and buoyancy frequency are shown for the upper (100-m) water column, as measured by glider RU06. Temperature ranged from 0.0 to -1.5°C (A); salinity showed a range of 0.3 (B); chlorophyll fluorescence showed a range of 30 mg m^{-3} (C); and buoyancy frequency (s^{-2}) ranged in magnitude two-fold. The numbers along the top (A) are the markers of glider segments identified on the yellow line in Figure 1.

doi: 10.12952/journal.elementa.000073.f003

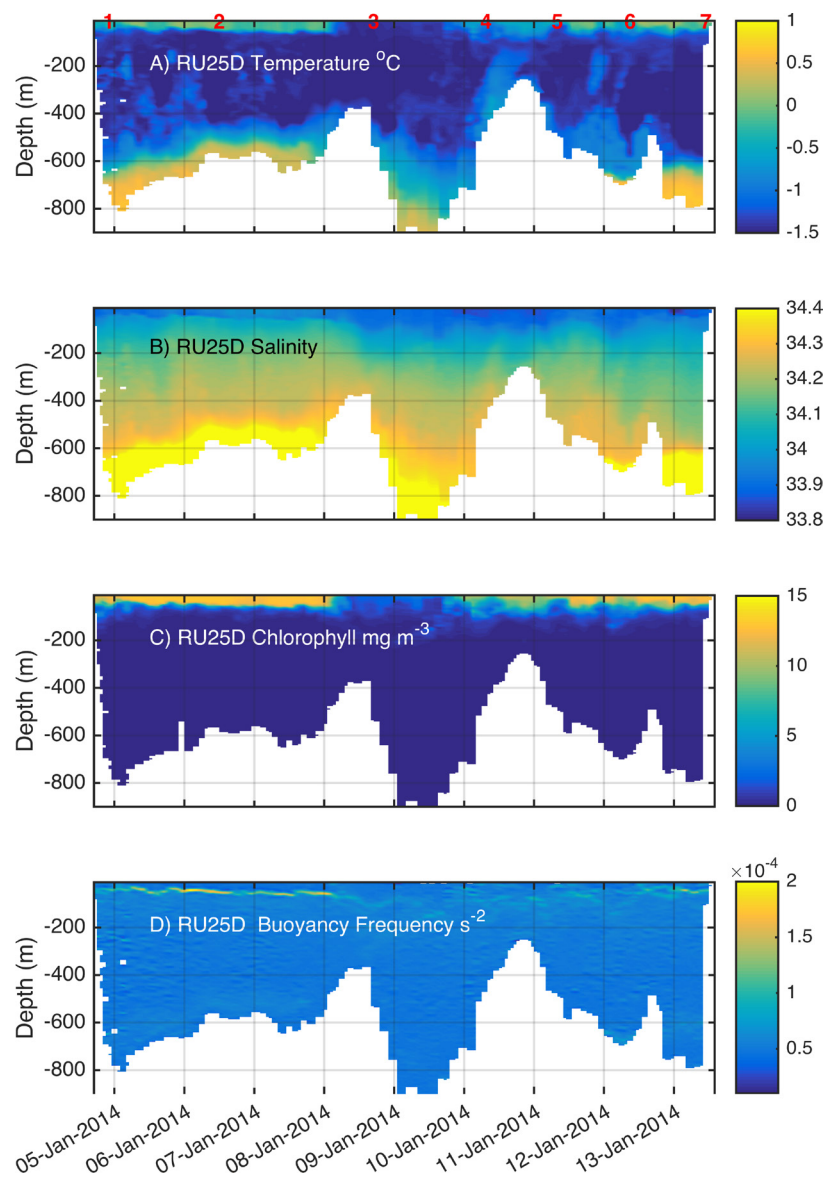


Figure 4

The full water column data collected by the deep-water glider during the KOPRI expedition.

Temperature, salinity, chlorophyll fluorescence and buoyancy frequency are shown throughout the water column, as measured by deep-water Webb glider RU25D. Temperature ranged from 1.0 to -1.5°C (A); salinity showed a range of 0.6 (B); chlorophyll fluorescence showed a range of 30 mg m^{-3} (C); and the buoyancy frequency (s^{-2}) calculated from the glider data ranged in magnitude greater than two-fold (D). The numbers along the top (A) are the markers of glider mission segments identified on the red line in Figure 1.

doi: 10.12952/journal.elementa.000073.f004

During ASPIRE, the ship and glider observed similar flow patterns. The depth-averaged currents from RU06 indicated the upper 100 m was characterized by low mean northward flow of 0.056 m s^{-1} and a mean east–west flow of -0.048 m s^{-1} (Figure 6, top panel) originating from the Dotson Ice Shelf. The shipboard along-shelf ADCP transect confirmed northward flow in the upper 100 m (Figure 7) with current speeds ranging from 0.15 to 0.05 m s^{-1} , similar in magnitude to the depth-averaged currents measured by the glider. The deeper current velocities measured by the ship showed depth dependence and spatial variability (Figure 7). At the eastern edge of the along-shelf transect, subsurface water ($> 200\text{ m}$) flowed south towards the ice sheet. On the western edge, bottom waters associated with a shallowing bathymetry showed subsurface waters ($> 200\text{ m}$) with a northward flow ($> 0.25\text{ m s}^{-1}$) associated with a topographic high. During most of the ASPIRE glider deployment, wind levels were consistent in direction and velocity; except during a few hours at the start of deployment, winds were consistently less than 10 m s^{-1} . Therefore, significant regional shifts in the upper ocean circulation were not likely driven by significant changes in weather forcing.

During the KOPRI cruise, RU25D encountered mean offshore flow relative to the Dotson Ice Shelf in the northwestern regions of the study area (Figure 8). Potential outflow of the deeper mCDW was observed on the western flank of the canyon during the KOPRI cruise. This outflow was seen as a filament of higher temperature water on the canyon edge (Figure 4, between segment 4 and 5 denoted at the top of panel A), located below 200-m water depth, and, like the ASPIRE ADCP sections, was associated with a shallowing of the seafloor. Generally, tidal currents were small relative to glider dead-reckoned velocities and thus were

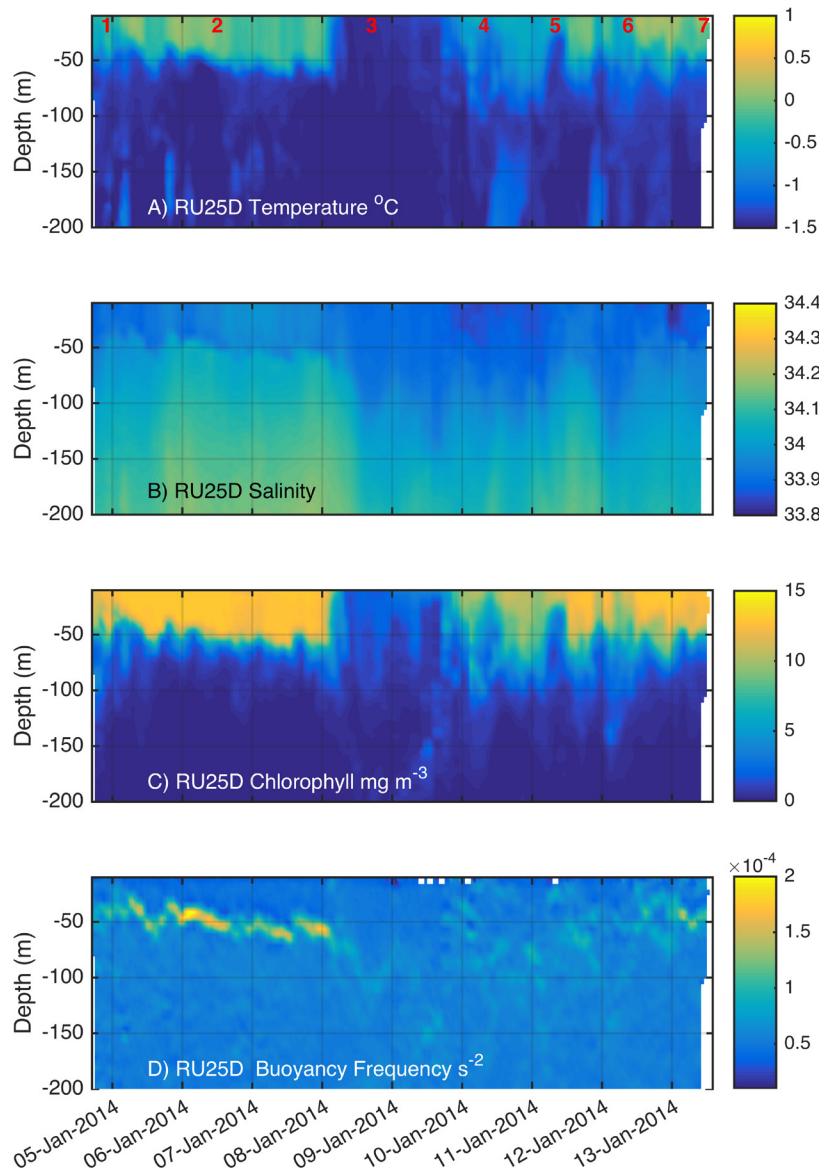


Figure 5

The upper 200-m water column data collected by the deep-water glider during the KOPRI expedition.

Temperature, salinity, chlorophyll fluorescence and buoyancy frequency are shown for the upper 200 m of the water column, as measured by deep-water Webb glider RU25D. Temperature ranged from of 0.0 to -1.5°C (A); salinity showed a range of 0.3 (B); chlorophyll fluorescence showed a range of 30 mg m^{-3} (C); and the buoyancy frequency (s^{-2}) calculated from the glider data ranged in magnitude just under two-fold (D). The numbers along the top (A) are the markers of glider mission segments identified on the red line in Figure 1.

doi: 10.12952/journal.elementa.000073.f005

not considered to greatly impact interpretation of mean flow patterns as derived from the glider and ship transects (Figures 6 and 8).

Bio-optical properties of the Amundsen Sea Polynya

Both the ASPIRE and KOPRI cruises coincided with the development of the phytoplankton spring/summer bloom (Figure 9). The timing of the peak phytoplankton concentrations in January was consistent with past studies (Arrigo et al., 2012). In both years, blooms were concentrated over deep water with lower phytoplankton biomass observed near the ice edge and on the shallower banks to the north (Figure 9). Satellite imagery indicated low biomass adjacent to the ice shelf consistent with ship and glider data; therefore, the land adjacency effects in the satellite imagery likely did not account for low values nearshore.

During ASPIRE, the RU06 mission was conducted when satellite-derived chlorophyll *a* concentrations (8-day average) ranged from < 1 to 10 mg m^{-2} (Figure 9). Highest phytoplankton biomass was found at the northern edge of the seafloor canyon, with lower levels on the northern polynya sea ice edge and bordering the Dotson and Getz ice shelves. By the end of the deployment, MODIS imagery showed that chlorophyll biomass had increased by ten-fold in the region (Figure 9). Glider chlorophyll estimates ranged from 1 to $15\text{ mg chlorophyll } a\text{ m}^{-3}$, which was similar to satellite estimates. During the KOPRI expedition, the blooms were spatially extensive with higher biomass observed throughout the same northern sector of the polynya

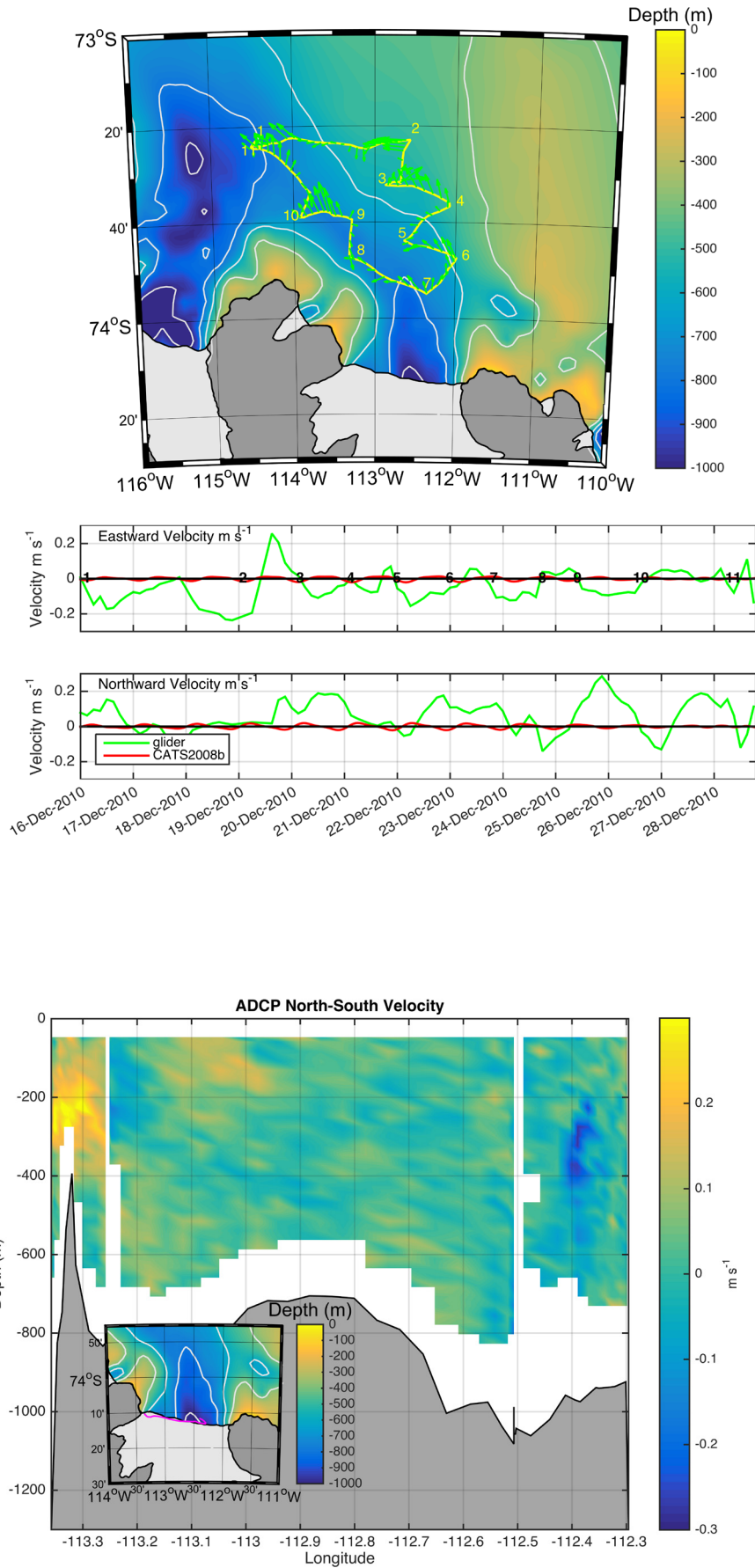


Figure 6

The depth-averaged current velocity and directional components estimated from the ASPIRE glider experiment.

The current velocity representing the average for the upper 100 m of the water column in austral summer 2010–2011 is shown for the study region, with the eastward and northward velocity components derived from the glider (green line) and modeled for the tides (red line). Numbers on the map and in the eastward velocity panel indicate segments of the glider mission presented in Figure 1.

doi: 10.12952/journal.elementa.000073.f006

Figure 7

The water-column current velocities near Dotson Ice Shelf, measured from the ship-mounted ADCP.

Current velocities (color scale in m s^{-1}) are shown throughout the water column measured by the ship-mounted acoustic doppler current profiler (ADCP) during the ASPIRE cruise. The inset shows the location of the ship transect (purple line) along the ice shelf for the plotted ADCP data.

doi: 10.12952/journal.elementa.000073.f007

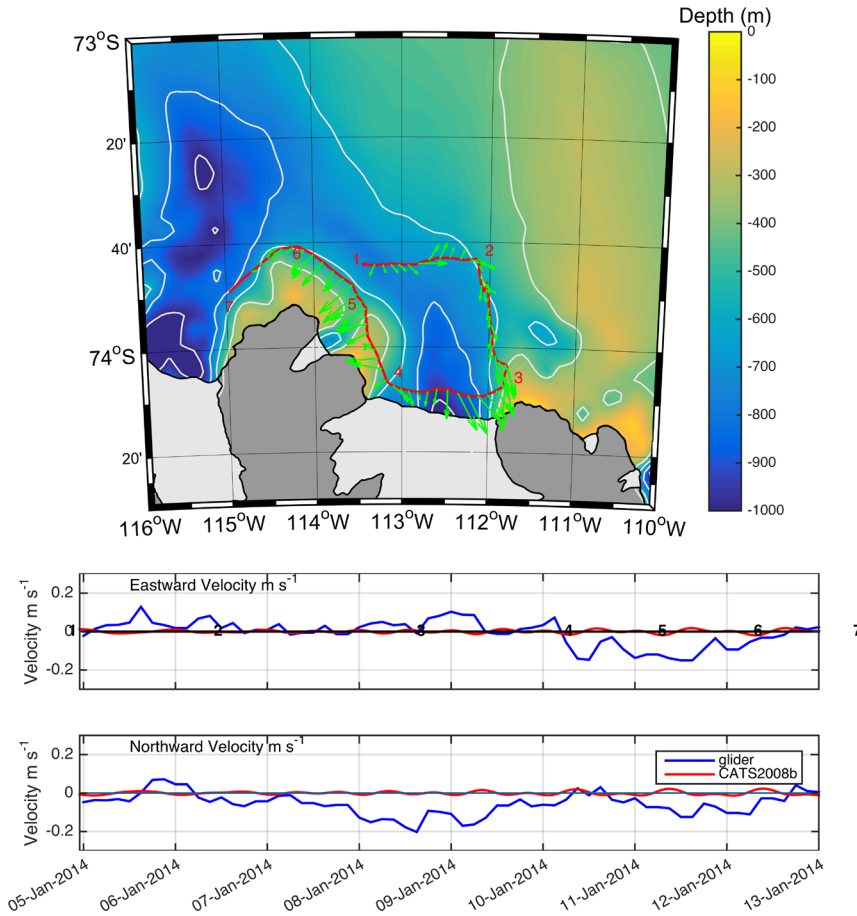


Figure 8

The depth-averaged current velocity and directional components estimated from the KOPRI glider experiment.

The current velocity representing the average for the upper 1000 m of water column in austral summer 2013–2014 is shown for the study region, with the eastward and northward velocity components derived from the glider (green line) and modeled for the tides (red line). Numbers on the map and in the eastward velocity panel indicate segments of the glider mission presented in Figure 1.

doi: 10.12952/journal.elementa.000073.f008

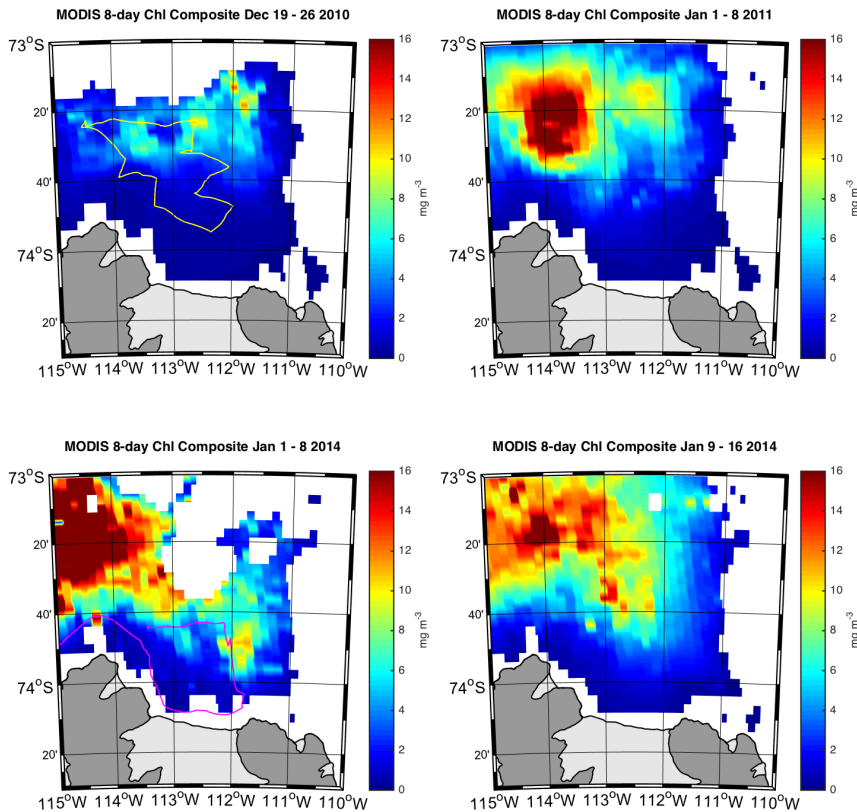


Figure 9

Satellite-derived chlorophyll estimates for the ASPIRE and KOPRI cruises.

Estimates of chlorophyll concentration (mg m^{-3}) based on MODIS-AQUA 8-day average ocean color images are shown for the study region. The yellow and red lines indicate the flight paths of the glider deployments.

doi: 10.12952/journal.elementa.000073.f009

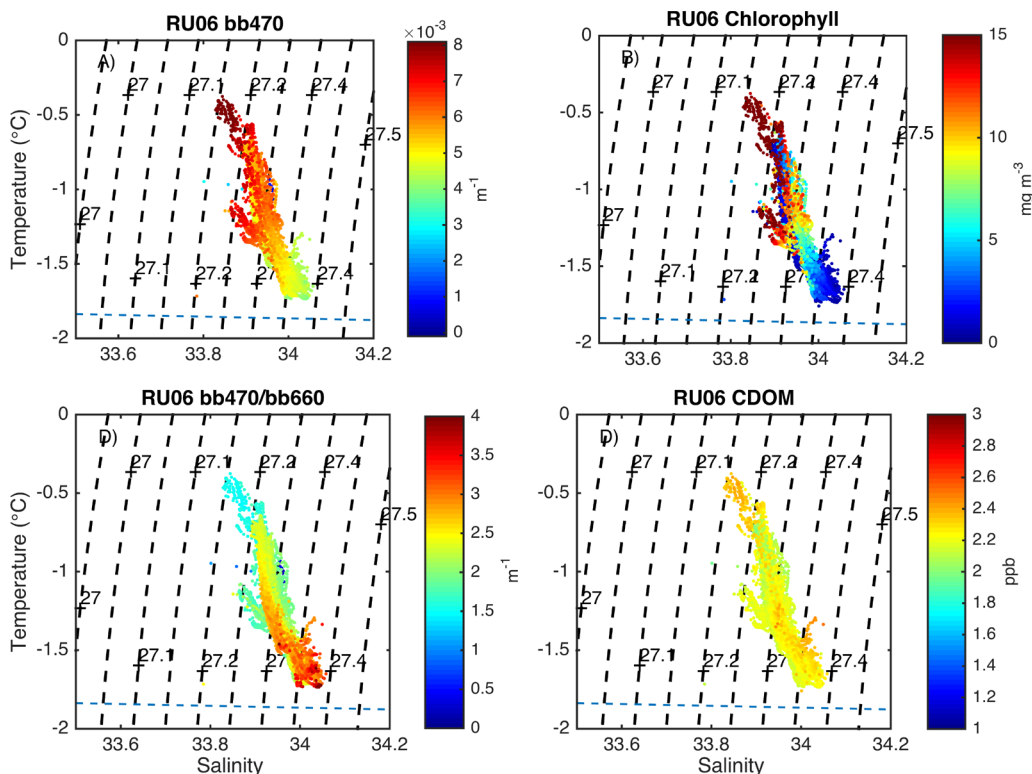


Figure 10

Bio-optical properties in temperature-salinity space measured by a 100-m glider experiment during the ASPIRE cruise.

Water column properties measured by Webb glider RU06 over a 100-m deployment are presented as a function of temperature and salinity: (A) optical backscatter at 470 nm (bb470 nm); (B) chlorophyll estimates (mg m^{-3}) from fluorescence; (C) the ratio of 470 to 880 nm optical backscatter (bb470/bb660); and (D) the fluorescence of colored dissolved organic matter (CDOM).

doi: 10.12952/journal.elementa.000073.f010

with the peak concentrations occurring in the first week of January (Figure 9B). The bloom appeared to have begun prior to the deployment of the glider with biomass remaining high by mid-January (Figure 9).

Glider surveys during ASPIRE indicated phytoplankton and particle concentrations were highest in warm (-1 to -0.5°C) lower salinity (< 34) AASW (Figures 10). In contrast, CDOM fluorescence indicated relatively uniform distributions across the temperature and salinity range encountered by the glider; therefore, the CDOM fluorescence did not have much power in discriminating water masses in this region. This finding was consistent with results from the Aaron expedition, when water masses were less well discriminated by CDOM compared to optical backscatter or oxygen data (Figure 11). Consistent with ASPIRE, during the Aaron cruise the highest values of optical backscatter were observed in the warm low saline waters (Figure 11). Fluorescence-based estimates of chlorophyll were > 10 -fold higher in warmer and lower saline surface waters. Chlorophyll fluorescence measurements indicated concentrations $> 15 \text{ mg m}^{-3}$. Chlorophyll fluorescence at ASPIRE glider recovery (same location after 13 d; Figure 12) showed a 5-fold increase relative to when the glider was deployed. This increase was consistent with the increasing chlorophyll concentrations observed in the satellite imagery (Figure 9). While chlorophyll increased dramatically, water temperature increased by $< 0.5^\circ\text{C}$ with a corresponding decrease of salinity by 0.1, suggesting a water mass with similar hydrographic features as when deployed. During the deployment there were steady, low wind speeds (10 m s^{-1}) which, combined with the depth-averaged flow measured by the glider, suggests flow from the low biomass waters near the ice sheet to the high biomass waters within the polynya. Given the minor shifts in water properties and transport, if we assume biomass accumulation represents the net growth rate of the phytoplankton, this observed increase translates to a net growth rate of $\sim 0.10 \text{ d}^{-1}$. During the ASPIRE cruise deckboard incubations of natural phytoplankton populations over a range of modified light levels and micronutrient conditions exhibited growth rates that ranged from 0.07 to 0.28 d^{-1} (Alderkamp et al., 2015). Lowest growth rates were observed for low light (1% light incubation levels) and low iron (Fe) conditions consistent with the ambient conditions of the AASW (Alderkamp et al., 2015).

High phytoplankton biomass in the AASW resulted in extremely turbid surface waters. The depth of the 1% light level ranged from 5 to 40 m during ASPIRE, as measured with the CTD rosette and modeled based on chlorophyll inputs into the Hydrolight model. The high biomass layers ranged in thickness from 20 to 50 m, consistent with the depth of the upper mixed layer. The fluorescence estimates of chlorophyll showed little variability in the upper mixed layer. Thus, given the high biomass and depth of the upper mixed layer, the majority of the phytoplankton biomass resided well below the 1% light level at any given time. Photosynthesis-irradiance curves indicated the light saturation intensity for photosynthesis (E_k) ranged from 37 to $67 \mu\text{mol photons m}^{-2} \text{ s}^{-1}$ (Alderkamp et al., 2015), which was consistent with low-light-acclimated phytoplankton populations when compared to average water column measurements of E_k in other pelagic

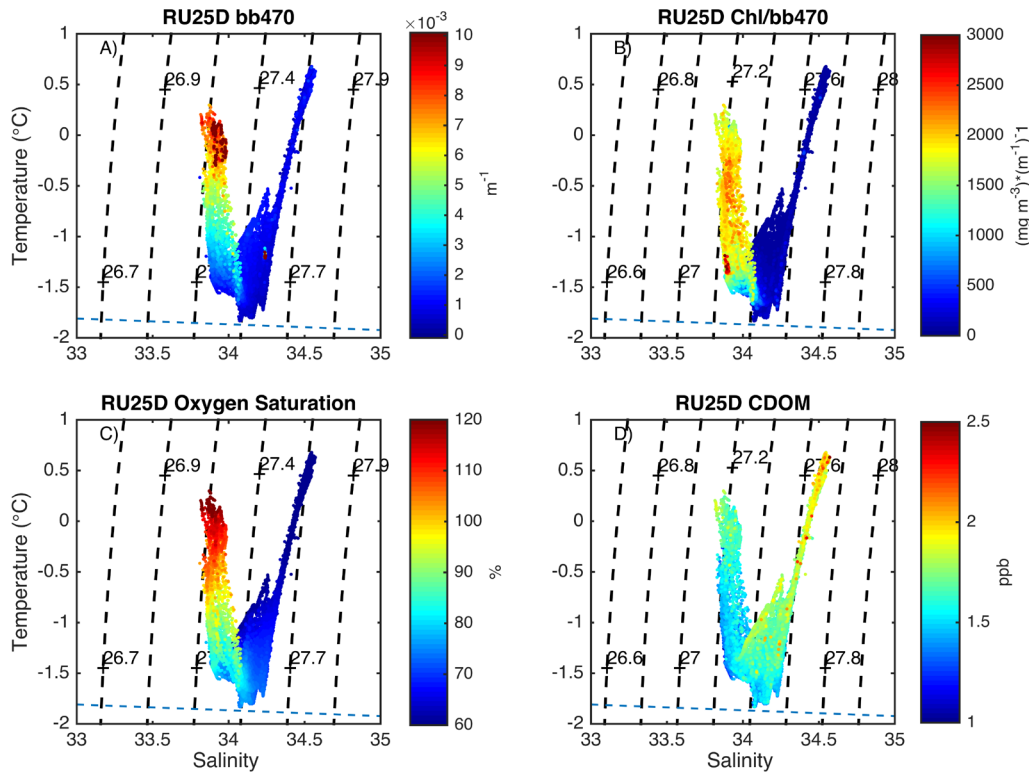


Figure 11

Bio-optical properties in temperature-salinity space measured by a 1000-m glider experiment during the KOPRI expedition.

Water column properties measured by Webb glider RU25D over a 1000-m deployment are presented as a function of temperature and salinity: (A) optical backscatter at 470 nm (bb470); (B) the ratio of chlorophyll from fluorescence to backscatter at 470 nm ($\text{mg m}^{-3}/\text{bb470}$); (C) the oxygen concentration (% saturation); and (D) the fluorescence of colored dissolved organic matter (CDOM).

doi: 10.12952/journal.elementa.000073.f011

and coastal locations in the Southern Ocean (Moline et al., 1998). While low salinity AASW was associated with regions of high phytoplankton biomass, it was not a guarantee of high phytoplankton biomass. During the KOPRI expedition high biomass was observed only when low salinity surface waters were confined to < 50 m. Near and along the ice edge, phytoplankton biomass was low within the upper 150 m despite the observed lower salinity (Figures 3, 5). Here, low water column stability confirmed the critical requirement of light in contributing to the phytoplankton blooms. There was a significant relationship with the depth of the upper mixed layer as defined by the maximum N^2 and the mean chlorophyll in the upper water column during both the ASPIRE and KOPRI expeditions (Figure 13; RU06 $R^2 = 0.43$ and p-value

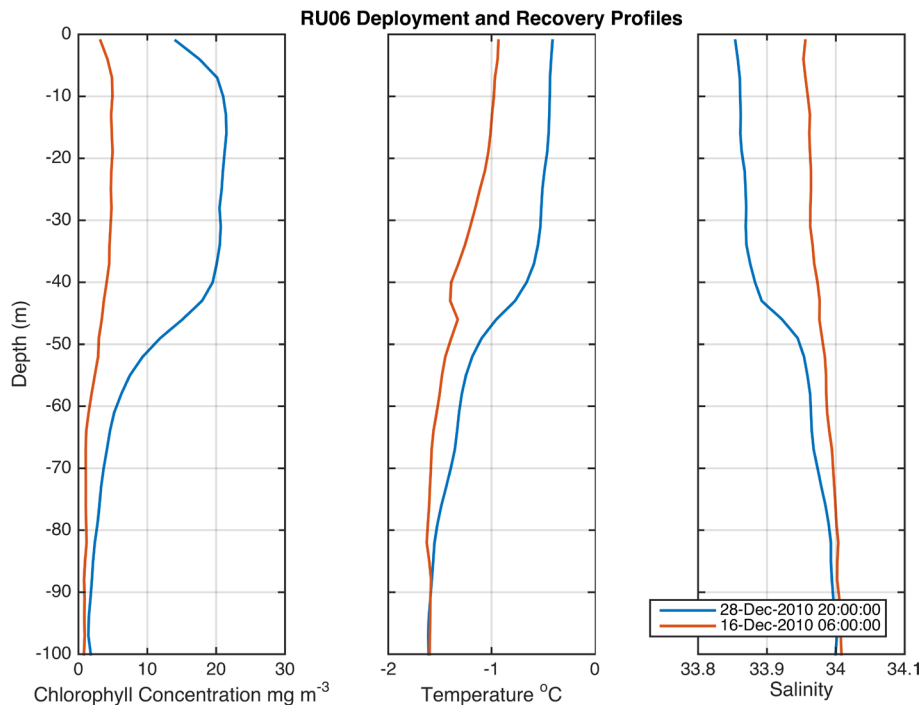


Figure 12

Depth profiles of chlorophyll fluorescence, temperature, and salinity at time of glider deployment and recovery.

The chlorophyll fluorescence (mg m^{-3}), temperature ($^{\circ}\text{C}$), and salinity are shown as a function of depth for the deployment (green line) and recovery (blue line) of Webb Slocum glider RU06. The deployment and recovery locations were at the same geographic location ($73^{\circ}23'12.15''\text{S}$ and $114^{\circ}26'04.91''\text{W}$).

doi: 10.12952/journal.elementa.000073.f012

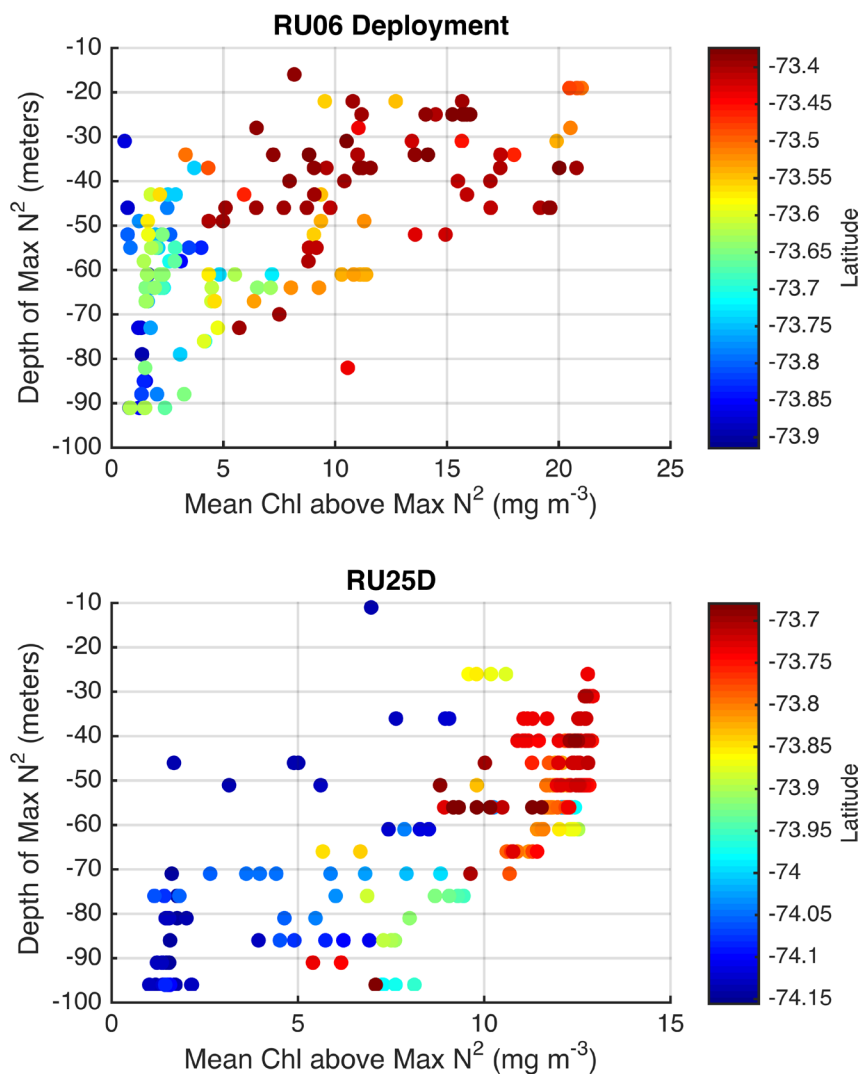


Figure 13

Relationship between depth of maximum water column buoyancy frequency (N^2) and mean chlorophyll concentration.

The relationship between the depth of maximum water column buoyancy frequency (N^2) and the mean chlorophyll a concentration (mg m^{-3}) is shown for the water column above the maximum N^2 depicted in Figures 4 and 5. The colors indicate the latitude of the water column measurements. Red colors generally indicate distance away from the ice shelf.

doi: 10.12952/journal.elementa.000073.f013

< 0.001, RU25D $R^2 = 0.59$ and p -value < 0.001). Higher chlorophyll was associated with lower latitudes (Figure 13) located offshore the ice edge (Figure 1B). The higher N^2 associated with the offshore waters was associated with increased solar warming of surface waters and the increased inputs of freshwater from sea ice melt (Alderkamp et al., 2015).

During ASPIRE, bio-optical data suggested that the nature of the particulate matter was unique in the lower salinity surface water compared to high salinity surface water. While fluorescence-based phytoplankton biomass estimates correlated with optical backscatter (for RU06 and RU25D, $R^2 = 0.92$ and 0.90 , respectively, p -value < 0.001), there was variability in the chlorophyll/backscatter and spectral backscatter ratios (Figure 10, 11). The spectral optical backscatter ratio (470 nm/660 nm) was lower in the AASW. The portions of the water column associated with high values of optical backscatter at 470 nm had low spectral backscatter ratios (470 nm/660 nm; Figure 10). In the high backscatter regions, the 20–30% range in the spectral ratio reflected a flattening in the backscatter spectrum, indicating either a change in the particle size distribution or a change in the organic/inorganic make-up of the particles (Boss et al., 2004). Furthermore, the variability in backscatter spectra suggests that it would be difficult to convert the backscatter data to a particle concentration without information on the particle type and size distribution (Boss et al., 2004). Pigment analyses revealed that the high biomass waters were dominated by prymnesiophyte algae, as indicated by HPLC measurements of 19'-hexanoyfucoxanthin. Microscopic examination identified *Phaeocystis pouchetti* as the dominant species present. The low chlorophyll concentrations were characterized by diatom communities, as indicated by the presence of fucoxanthin. These shifts were consistent with the spatial variability in the optical backscatter ratio.

Discussion

Understanding the physical regulation of primary productivity and community structure along ice shelves and polynyas is critical to understanding the regional ecology and biogeochemistry. Polynyas in the Amundsen Sea region are characterized by large phytoplankton blooms (Arrigo et al., 2012; Lee et al., 2012) and are experiencing change due to climate forcing (Holland, 2014). Phytoplankton studies in key polynyas to date have focused on defining the relative importance of nutrient versus light regulation (Lee et al., 2012), with numerous efforts focusing on the importance of iron (Fe) in driving phytoplankton growth in polynyas (Buma et al., 1991; Sedwick and DiTullio, 1997; Sedwick et al., 2000; Tagliabue and Arrigo, 2005).

Deckboard incubations during ASPIRE confirmed the importance of Fe in promoting accelerated growth in phytoplankton (Alderkamp et al., 2015). There are several potential sources of Fe reflecting a range of ocean-ice sheet-seafloor interactions. The potential sources of Fe include basal melting of glaciers and beneath ice shelves, sediment resuspension within the sub-glacial cavity and at grounding lines, and direct input from calved icebergs (Gerringa Loes et al., 2012; Yager et al., 2012). While these sources are sufficiently large to support large phytoplankton blooms (Sherrell et al., 2015), deckboard incubations suggest increased input of Fe could increase primary productivity by a factor of 1.7 (Alderkamp et al., 2015).

The mCDW subsurface outflow from the ice sheet appears to be a major source of dissolved and particulate iron to the polynya (Gerringa Loes et al., 2012; Sherrell et al., 2015). Driven by Coriolis and pressure gradient forces, the relatively dense CDW travels along-isobath toward the ice shelves with the coastline to the left of the flow. This warm water mass affects the glaciers and ice shelves, melting ice and forming a modified CDW (mCDW) and meltwater mixture (Jenkins, 1999; Walker et al. 2007; Jenkins and Jacobs, 2008; Jenkins et al., 2010; Jacobs et al., 2011). Presumably the meltwater input increases buoyancy of the mCDW, causing upwelling, while the Coriolis force drives outflows on the southern and western sides of the ice shelves dependent on bathymetric orientation. The micronutrients associated with outflow can fuel productivity if mixing carries the deeper water into the euphotic zone. It has been hypothesized that transport of subsurface water to the surface is driven by horizontal diffusivity (Gerringa Loes et al., 2012), advective eddy transport (e.g., Årthun et al., 2013), mixing along the Dotson trough (St-Laurent et al., 2013), and wind- and iceberg-induced mixing (Randall-Goodwin et al., 2015). Given the slow, calculated *in situ* and deckboard growth rates of the phytoplankton and the observed high biomass, injection of nutrients through destratification of the full water column followed by stratification and subsequent regrowth is unlikely. The injection of micronutrients would thus likely be dominated by horizontal and vertical advection and diffusive mixing. Observations suggest that dissolved iron- and meltwater-rich deep water shoals from the basal ice shelf towards the central polynya and likely supports the bloom there (Sherrell et al., 2015). Recent results in the ice shelf outflow region, showing decreasing optical backscatter with proximity to the seafloor, suggest that particulate matter, which had a linear relationship with meltwater concentration, was sourced from the overlying glacier rather than resuspended sediment (Miles et al., 2015b).

The robust relationship between water column stability and chlorophyll concentration suggests the importance of the light environment in driving phytoplankton standing stock in the ASP. The high concentrations of phytoplankton encountered in this polynya indicate an extremely productive system. Productivity rates are similar to the high productivity rates found along the West Antarctic Peninsula (WAP; Ducklow et al., 2007), with the contrast that along the WAP the high productivity regions are associated with diatoms (Hart, 1942; Moline et al., 2004; Vernet et al., 2008; Montes-Hugo et al., 2009). The high productivity rates associated with *Phaeocystis* in the ASP are consistent with the Ross Sea (Smith et al., 1998, 2003). Additionally, the high concentrations of chlorophyll encountered during the ASPIRE and KOPRI cruises are consistent with past ship (Lee et al., 2012) and satellite studies (Arrigo et al., 2012). Given the high biomass in these waters, satellite estimates of chlorophyll would underestimate the overall biomass significantly, as the depth of the satellite section would span only the upper few meters of the water column, missing the majority of the phytoplankton biomass (Kirk, 2011).

The ASP with its high biomass conditions represents a unique environment in which the interplay between nutrient availability and light limitation is extremely complex (Dubinsky and Schofield, 2009). Phytoplankton populations are capable of photoacclimating to low light conditions and measured photosynthesis-irradiance curves during ASPIRE indicated the cells were low light-adapted (Alderkamp et al., 2015); however cells were still often chronically light-limited. This was especially true as the upper mixed layer was often deeper than the euphotic zone (defined as the 1% light level). The net result is that in the high biomass waters any small shift in the mean position of phytoplankton in the water column (meters) could shift a cell from being light-saturated to being light-limited; therefore, cell motility and/or mixing within the turbid upper mixed layer waters must play a predominant role in determining the overall water column productivity and corresponding growth of the phytoplankton (Kroon and Thoms, 2006; Dubinsky and Schofield, 2009; Schofield et al., 2013b).

Given that a relatively constant biomass of phytoplankton spanned the upper mixed layer (Figure 12) which was often over 10-fold deeper than the depth of the 1% light level, active movement of the phytoplankton in the upper mixed layer might be required to maintain growth rates in upper mixed layer. While

many phytoplankton species exhibit significant movement through swimming (Blasco, 1978) and/or buoyancy regulation (Walsby et al., 1997), there is no evidence that *Phaeocystis* exhibits capabilities for significant vertical motility. The few available laboratory studies on *Phaeocystis* suggest that cells are either neutrally or slightly negatively buoyant under light-limiting conditions (Wang and Tang, 2010). Although these studies were not conducted on the Antarctic species encountered during the ASPIRE and KOPRI expeditions, it appears that the rate of mixing within the upper mixed layer and not cell motility is critical to supporting the observed accumulation of phytoplankton biomass.

Phytoplankton photosynthesis can be extremely efficient in turbid conditions if mixing promotes the “fluctuating light effect” (Phillips and Myers, 1954; Myers, 1994). The “fluctuating light effect” describes when phytoplankton exposed to dynamic light intensities can have photosynthesis rates and biomass yields that are higher than cells grown under a constant photon dose, due to differences in the slow kinetics of the xanthophyll cycle relative to the mixing rate (minutes-hours; Demmig et al., 1987; Demmig-Adams, 1990), thereby allowing cells to operate at maximal photosynthetic efficiencies. Past studies in turbid plumes have demonstrated that not accounting for mixing in the upper mixed layer could lead to large errors (as large as 40%) for traditional static biological measurements of phytoplankton productivity (Schofield et al., 2013b). Therefore, improved understanding of the phytoplankton ecology will require measurements of turbulent mixing rates to define the light environment for cells within the upper mixed layer.

Conclusions

Recent reports highlight that glacial melt in the Amundsen Sea will continue for the foreseeable future (Thoma et al., 2008; Holland, 2014). Continuing glacial melt will increase the delivery of low salinity water into the Amundsen Sea Polynya (Hellmer, 2004), which will have biogeochemical ramifications through potentially increasing the overall productivity of this polynya (Arrigo et al., 2012) if the physical integrity of the system is otherwise maintained. Glider results from two different expeditions support this interpretation, as low salinity plumes associated with pycnoclines shallower than 50 m corresponded to regions of highest phytoplankton biomass. Additionally, the overall regulation of the phytoplankton biomass must be strongly influenced by mixing within the upper mixed layer, as mixing determines the proportion of the community experiencing chronic light limitation. Therefore, there is a critical need to quantify mixing within the AASW to better understand the injection of iron into surface waters and to model the light environment in a turbid high-biomass environment.

References

- Alderkamp AC, Mills MM, Van Dijken GL, Laan P, Thuyr oczy C-E, et al. 2012. Iron from melting glaciers fuels phytoplankton blooms in the Amundsen Sea (Southern Ocean): Phytoplankton characteristics and productivity. *Deep-Sea Res Pt II* 71–76: 32–48. doi: 10.1016/j.dsr2.2012.03.005.
- Alderkamp A, van Dijken GL, Lowry KE, Connelly TL, Lagerstrom M, et al. 2015. Fe availability drives phytoplankton photosynthesis rates in the Amundsen Sea Polynya, Antarctica. *Elem Sci Anth* 3. doi: 10.12952/journal.elementa.000043.
- Arrigo KR, Robinson DH, Worthen DL, Dunbar RB, DiTullio GR, et al. 1999. Phytoplankton community structure and the drawdown of nutrients and CO₂ in the Southern Ocean. *Science* 285(5400): 365–367. doi: 10.1126/science.283.5400.365.
- Arrigo KR, van Dijken GL. 2003. Phytoplankton dynamics within 37 Antarctic coastal polynyas. *J Geophys Res* 108(c8): 3271. doi: 10.1029/2002JC001739.
- Arrigo KR, van Dijken GL, Long MC. 2008. The coastal Southern Ocean: A strong anthropogenic CO₂ sink. *Geophys Res Lett* 35: 121602. doi: 10.1029/2008GL035624.
- Arrigo KR, Lowry KE, van Dijken GL. 2012. Annual changes in sea ice and phytoplankton in polynyas of the Amundsen Sea, Antarctica. *Deep-Sea Res Pt II* 71: 5–15. doi: 10.1016/j.dsr2.2012.03.006.
-  rthun M, Holland PR, Nicholls KW, Feltham DL. 2013. Eddy-driven exchange between the open ocean and a sub-ice shelf cavity. *J Phys Oceanogr* 43: 2372–2387.
- Assmann KM, Jenkins A, Shoosmith DR, Walker DP, Jacobs SS, et al. 2013. Variability of Circumpolar Deep Water transport onto the Amundsen Sea continental shelf through a shelf break trough. *J Geophys Res-Oceans* 118(12): 6603–6620. doi: 10.1002/2013JC008871.
- Blasco D. 1978. Observations on the diel migration of marine dinoflagellate off the Baja California coast. *Mar Biol* 46: 41–47.
- Boss E, Pegau W. 2001. Relationship of light scattering at an angle in the 524 backward direction to the backscattering coefficient. *Appl Optics* 40(30): 5503–5525. doi: 10.1364/AO.40.005503.
- Boss E, Pegau SW, Lee M, Twardowski MS, Shybanov E, et al. 2004. The particulate backscattering ratio at LEO 15 and its use to study particle composition and distribution. *J Geophys Res* 109: C01014. doi: 10.1029/2002JC001514.
- Buma AGJ, De Baar HJW, Nolting RF, Van Bennekom AJ. 1991. Metal enrichment experiments in the Weddell-Scotia Seas - Effects of iron and manganese on various plankton communities. *Limnol Oceanogr* 36: 1865–1878.
- Caron DA, Dennett MR, Lonsdale DJ, Moran DM, Shalapyonok L. 2000. Microzooplankton herbivory in the Ross Sea, Antarctica. *Deep-Sea Res Pt II* 47: 3249–3272.
- Davis R, Eriksen C, Jones C. 2003. Autonomous buoyancy-driven underwater gliders, in Griffiths G, ed., *Technology and Applications of Autonomous Underwater Vehicles*. London: Taylor & Francis: pp. 37–58.
- Demmig B, Winter K, Kruger A, Czygan FC. 1987. Photoinhibition and zeaxanthin formation in intact leaves: A possible role of the xanthophyll cycle in the dissipation of excess light energy. *Plant Physiol* 84: 218–224.

- Demmig-Adams B. 1990. Carotenoids and photoprotection in plants: a role for the xanthophyll zeaxanthin. *Biochim Biophys Acta* **1020**: 1–24.
- Dubinsky Z, Schofield O. 2009. From the light to the darkness: Thriving at the light extremes in the oceans. *Hydrobiologia* **639**(1): 153–171. doi: 10.1007/s10750-009-0026-0.
- Ducklow HW, Baker KS, Martinson DG, Quetin LB, Ross RM, et al. 2007. Marine pelagic ecosystems: The West Antarctic Peninsula. *Philos Trans R Soc London* **362**: 67–94. doi: 10.1098/rstb.2006.1955.
- Fragoso GM, Smith WO. 2012. Influence of hydrography on phytoplankton distribution in the Amundsen and Ross Seas, Antarctica. *J Marine Syst* **89**: 19–29. doi: 10.1016/j.jmarsys.2011.07.008.
- Glenn SM, Jones C, Twardowski M, Bowers L, Kerfoot J, et al. 2008. Glider observations of sediment resuspension in a Mid-Atlantic Bight fall transition storm. *Limnol Oceanogr* **53**(5.2): 2180–2196.
- Gerringa Loes JA, Alderkamp A, Lann O, Thuróczy CE, De Baar HJW, et al. 2012. Iron from melting glaciers fuels the phytoplankton blooms in Amundsen Sea (Southern Ocean): Iron biogeochemistry. *Deep-Sea Res Pt II* **71**: 16–31. doi: 10.1016/j.dsr2.2012.03.007.
- Gruber N, Gloor M, Mikaloff-Fletcher SE, Dutkiewicz S, Follows M, et al. 2009. Oceanic sources and sinks for atmospheric CO₂. *Global Biogeochem Cy* **23**: GB1005. doi.org/10.1029/2008GB003349.
- Ha HK, Wählin AV, Kim TW, Lee SH, Lee JH, et al. 2014. Circulation and modification of warm deep water on the central Amundsen Shelf. *J Phys Oceanogr* **44**(5): 1493–1501. doi: 10.1175/JPO-D-13-0240.1.
- Hart TJ. 1942. Phytoplankton periodicity in Antarctic surface waters. *Discovery Rep* **21**: 261–356.
- Hellmer HH. 2004. Impact of Antarctic ice shelf basal melting on sea ice and deep ocean properties. *Geophys Res Lett* **31**: L10307. doi: 10.1029/2004GL019506.
- Holland PR. 2014. The seasonality of Antarctic sea ice trends. *Geophys Res Lett* **41**: 4230–4237. doi: 10.1002/2014GL060172.
- Holm-Hansen O, Lorenzen C, Holmes RW, Strickland JDH. 1965. Fluorometric determination of chlorophyll in Chlorophyta, Chrysophyta, Phaeophyta, Pyrrophyta. *J Cons Perm Inter Explor Mer* **30**: 3–15.
- Jacobs SS, Jenkins A, Giulivi CF, Dutrieux P. 2011. Stronger ocean circulation and increasing melting under Pine Island Glacier ice shelf. *Nat Geosci* **4**: 519–523.
- Jenkins A. 1999. The impact of melting ice on ocean waters. *J Phys Oceanogr* **3**: 2370–2381.
- Jenkins A, Jacobs S. 2008. Circulation and melting beneath George VI Ice Shelf, Antarctica. *J Geophys Res* **113**(C4): C04013. doi: 10.1029/2007JC004449.
- Jenkins A, Dutrieux P, Jacobs S, McPhail SD, Perrett JR, et al. 2010. Observation beneath Pine Island Glacier in West Antarctica and implications for its retreat. *Nature Geosci* **3**(7): 468–472. doi: 10.1038/ngeo890.
- Johnson R, Strutton PG, Wright SW, McMinn A, Meiners KM. 2013. Three improved satellite chlorophyll algorithms for the Southern Ocean. *J Geophys Res* **118**: 1–10. doi: 10.1002/jgrc.20270.
- Kirk JTO. 2011. *Light and Photosynthesis in Aquatic Ecosystems*. New York: Cambridge University Press: 662 p.
- Kroon BM, Thoms S. 2006. From electron to biomass: A mechanistic model to describe phytoplankton photosynthesis and steady-state growth rates. *J Phycol* **42**(3): 593–609.
- Lee SH, Kim BK, Yun MA, Joo H, Yang EJ, et al. 2012. Spatial distribution of phytoplankton productivity in the Amundsen Sea, Antarctica. *Polar Biol* **35**(11): 1721–1733. doi: 10.1007/s00300-012-1220-5.
- Liss PS, Malin G, Turner SM, Holigan PM. 1994. Dimethyl sulphide and *Phaeocystis*: A review. *J Marine Syst* **5**(1): 41–53.
- Marshall GJ. 2007. Half-century seasonal relationships between the Southern Annular Mode and Antarctic temperatures. *Int J Climatol* **27**: 373–383. doi: 10.1002/joc.1407.
- Merckelbach LM, Briggs RD, Smeed DA, Griffiths G. 2008. Current measurements from autonomous underwater gliders, in *Proceedings of the IEEE/OEC/CMTIC Ninth Working Conference on Current Measurement Technology*: pp. 61–67.
- Miles T, Glenn SM, Schofield O. 2012. Spatial variability in fall storm induced sediment resuspension on the Mid-Atlantic Bight. *Cont Shelf Res*. doi: 10.1016/j.csr.2012.08.006.
- Miles T, Seroka G, Kohut J, Schofield O, Glenn SM. 2015a. Glider observations and modeling of sediment transport in Hurricane Sandy. *J Geophys Res Oceans*. doi: 10.1002/2014JC010474.
- Miles TN, Lee SH, Wählin A, Ha HK, Schofield O, Kim TW, Assmann K. 2015b. Observations of the Dotson Ice Shelf outflow: Implications for the iron fertilization of the Amundsen polynya. *Deep-Sea Res Pt II*. doi: 10.1016/j.dsr2.2015.08.008.
- Mobley CD. 1994. *Light and Water: Radiative Transfer in Natural Waters*. New York: Academic Press: 592 p.
- Moline MA, Claustre H, Frazer TK, Schofield O, Vernet M. 2004. Alteration of the food web along the Antarctic Peninsula in response to a regional warming trend. *Glob Change Biol* **10**: 1973–1980.
- Moline MA, Schofield O, Boucher NB. 1998. Photosynthetic parameters and empirical modeling of primary production in the Southern ocean. *Antarct Sci* **10**: 45–54.
- Montes-Hugo M, Doney SC, Ducklow HW, Fraser W, Martinson D, 2009. Recent changes in phytoplankton communities associated with rapid regional climate change along the Western Antarctic Peninsula. *Science* **323**: 1470–1473.
- Myers J. 1994. The 1932 experiments. *Photosynth Res* **40**: 303–310.
- Padman L, Fricker HA, Coleman R, Howard S, Erofeeva L. 2002. A new tide model for the Antarctic ice shelves and seas. *Ann Glaciol* **34**(1): 247–254.
- Phillips JN, Myers J. 1954. Growth rate of *Chlorella* in flashing light. *Plant Physiol* **29**: 152–161.
- Randall-Goodwin E, Meredith MP, Jenkins A, Yager PL, Sherrell RM, et al. 2015. Freshwater distributions and water mass structure in the Amundsen Sea Polynya region, Antarctica. *Elem Sci Anth* **3**: 000065. doi: 10.12952/journal.elementa.000065.
- Rignot E. 2008. Changes in West Antarctic ice stream dynamics observed with ALOS PALSAR data. *Geophys Res Lett* **35**: L12505. doi: 10.1029/2008GL033365.
- Rignot E, Jacobs S, Mouginot J, Scheuchi B. 2013. Ice-shelf melting around Antarctica. *Science* **341**(6143): 266–270. doi: 10.1126/science.1235798.
- Rudnick DL, Cole ST. 2011. On sampling the ocean using underwater gliders. *J Geophys Res* **116**. doi: 10.1029/2010jc006849.
- St-Laurent P, Klinck JM, Dinniman MS. 2013. On the role of the coastal troughs in the circulation of warm circumpolar deep water on Antarctic shelves. *J Phys Oceanogr* **43**: 51–64.

Phytoplankton in the Amundsen Sea Polynya

- Sarmiento JL, Gruber N, Brzezinski MA, Dunne JP. 2004. High-latitude controls of thermocline nutrients and low latitude biological productivity. *Nature* **427**: 56–60. doi: 10.1038/nature02127.
- Schofield O, Kohut J, Aragon D, Creed L, Graver J, et al. 2007. Slocum Gliders: Robust and ready. *J Field Robotics* **24**(6): 473–485. doi: 10.1009/rob.20200.
- Schofield O, Ducklow HW, Martinson DG, Meredith MP, Moline MA, et al. 2010. How do polar marine ecosystems respond to rapid climate change? *Science* **328**: 1520. doi: 10.1126/science.1185779.
- Schofield O, Ducklow H, Bernard K, Doney S, Fraser-Patterson D, et al. 2013a. Penguin biogeography along the West Antarctic Peninsula: Testing the canyon hypothesis with Palmer LTER observations. *Oceanography* **26**: 78–80.
- Schofield O, Moline MA, Cahill B, Frazer T, Kahl A, et al. 2013b. Phytoplankton productivity in a turbid buoyant coastal plume. *Cont Shelf Res* **63**: S138–S148. doi: 10.1016/j.csr.2013.02.00.
- Sedwick PN, DiTullio GR. 1997. Regulation of algal blooms in Antarctic shelf waters by the release of iron from melting sea ice. *Geophys Res Lett* **24**: 2515–2518.
- Sedwick PN, DiTullio GR, Mackey DJ. 2000. Iron and manganese in the Ross Sea, Antarctica: Seasonal iron limitation in Antarctic shelf waters. *J Geophys Res* **105**: 11321–11336.
- Sherrell RM, Lagerström M, Forsch K, Stammerjohn SE, Yager PL. 2015. Dynamics of dissolved iron and other bioactive trace metals (Mn, Ni, Cu, Zn) in the Amundsen Sea Polynya, Antarctica. *Elem Sci Anth*: in press for this Special Feature.
- Smith WO Jr, Carlson CA, Ducklow HW, Hansell DA. 1998. Growth dynamics of *Phaeocystis antarctica*-dominated plankton assemblages from the Ross Sea. *Mar Ecol-Prog Ser* **168**: 229–244.
- Smith WO Jr, Dennett MR, Mathot S, Caron DA. 2003. The temporal dynamics of the flagellated and colonial stages of *Phaeocystis antarctica* in the Ross Sea. *Deep-Sea Res Pt II* **50**: 605–618.
- Smith WO Jr, Shields AR, Peloquin JA, Catalano G, Tozzi S, et al. 2006. Interannual variations in nutrients, net community production, and biogeochemical cycles in the Ross Sea. *Deep-Sea Res Pt II* **53**: 815–833. doi: 10.1016/j.dsr2.2006.02.014.
- Stammerjohn S, Massom R, Rind D, Martinson D. 2012. Regions of rapid sea ice change: An inter-hemispheric seasonal comparison. *Geophys Res Lett* **39**: L06501. doi: 10.1029/2012GL050874.
- Stammerjohn SE, Maksym T, Massom RA, Lowry KE, Arrigo KR, et al. 2015. Seasonal sea ice changes in the Amundsen Sea, Antarctica, over the period of 1979–2014. *Elem Sci Anth* **3**: 000055. doi: 10.12952/journal.elementa.000055.
- Tagliabue A, Arrigo KR. 2005. Iron in the Ross Sea: 1. Impact on CO₂ fluxes via variation in phytoplankton functional group and non-Redfield stoichiometry. *J Geophys Res* **110**(C3): C03009. doi: 10.1029/2004JC002531.
- Thoma M, Jenkins A, Holland D, Jacobs S. 2008. Modelling circumpolar deep water intrusions on the Amundsen Sea continental shelf, Antarctic. *Geophys Res Lett* **35**: L18602. doi: 10.1029/2008GL034939.
- Vernet M, Martinson D, Iannuzzi R, Stammerjohn S, Kozlowski W, et al. 2008. Primary production within the sea-ice zone west of the Antarctic Peninsula: I—Sea ice, summer mixed layer, and irradiance. *Deep-Sea Res Pt II* **55**: 2068–2085.
- Wählin AK, Yuan X, Björk G, Nohr C. 2010. Inflow of warm Circumpolar Deep Water in the central Amundsen Shelf. *J Phys Oceanogr* **40**: 1427–1434. doi: 10.1175/2010JPO4431.1.
- Wählin AK, Muench RD, Arneborg L, Björk G, Ha HK, et al. 2012. Some implications of Ekman layer dynamics for cross-shelf exchange in the Amundsen Sea. *J Phys Oceanogr* **42**(9): 1461–1474. doi: 10.1175/jpo-d-11-041.1.
- Walker DP, Brandon MA, Jenkins A, Allen JT, Dowdeswell JA, et al. 2007. Oceanic heat transport onto the Amundsen Sea shelf through a submarine glacial trough. *Geophys Res Lett* **34**: L02602. doi: 10.1029/2006GL028154.
- Walsby AE, Hayes PK, Boje R, Stal LJ. 1997. The selective advantage of buoyancy provided by gas vesicles for planktonic cyanobacteria in the Baltic Sea. *New Phytol* **136**: 407–417.
- Wang X, Tang KW. 2010. Buoyancy regulation in *Phaeocystis globosa* Scherffel colonies. *Open Mar Biol J* **4**: 115–121.
- Wright SW, Jeffrey SW, Mantoura RFC, Llewellyn CA, Björnlan T, et al. 1991. Improved HPLC method for the analysis of chlorophylls and carotenoids from marine phytoplankton. *Mar Ecol-Prog Ser* **77**: 183–196.
- Xu Y, Cahill B, Wilkin J, Schofield O. 2012. Role of wind in regulating phytoplankton blooms on the Mid-Atlantic Bight. *Cont Shelf Res* **63**: S26–S35. doi: 10.1016/J.CSR.2012.09.011.
- Yager PL, Sherrell RM, Stammerjohn SE, Alderkamp AC, Schofield O, et al. 2012. ASPIRE: The Amundsen Sea Polynya International Research Expedition. *Oceanography* **25**(3): 40–53. doi: 10.5670/oceanog.2012.73.

Contributions

- Contributed to conception and design: OS, PY, RS, TM, SL
- Contributed to acquisition of data: TH, ER, RES
- Contributed to analysis and interpretation of data: OS, TM, ACA, PY, RS
- Contributed to draft and revised the article: OMS, TM, ACA, SLH, TH, ER, RES, RS, PY
- Approved and submitted version of publication: OS, PY

Acknowledgments

We thank the excellent support teams and ship crews of the RVIB Nathaniel B Palmer and the Aaron and the associated wider ASPIRE scientific teams. We also acknowledge the ongoing support from the great state of New Jersey.

Funding information

This project was funded by the National Science Foundation Office of Polar Programs, Antarctic Organisms and Ecosystems (ANT-0839069 to PY, ANT-0838995 to RS, ANT-0838975 to SS, ANT-0838995 to OS). Support was also provided by the KOPRI grant PP1502.

Competing interests

The authors declare no competing interests.

Data accessibility statement

Glider data can be accessed at a Thredds server: <http://tds.marine.rutgers.edu:8080/thredds/catalog/cool/glider/all/catalog.html> and at ERDDAP server at <http://erddap.marine.rutgers.edu/erddap/info/index.html?page=1&itemsPerPage=1000>

Copyright

© 2015 Schofield et al. This is an open-access article distributed under the terms of the Creative Commons Attribution License, which permits unrestricted use, distribution, and reproduction in any medium, provided the original author and source are credited.